Journal of Applied Polymer Science

Flame retardancy and mechanical properties of ferrum ammonium phosphate–halloysite/epoxy polymer nanocomposites

Yanmao Dong,[1,2] Brian Lisco,[2] Hao Wu,[3] Joseph H. Koo,[2] Mourad Krifa[4]

[1]Suzhou University of Science and Technology, School of Chemistry, Biology and Materials Engineering, 1 Kerui Road, Suzhou JS 215009, China

[2]Department of Mechanical Engineering, The University of Texas at Austin, 204 East Dean Keaton Street C2200, Austin, Texas 78712

[3]Materials and Science Program, The University of Texas at Austin, Austin, Texas 78712

[4]Department of Textiles and Apparel, The University of Texas at Austin, A270, Austin, Texas 78712

Correspondence to: Y. Dong (E-mail: dongyanmao0512@gmail.com)

ABSTRACT: To recycle the nitrogen (N) and phosphorus (P) from wastewater, ferrum ammonium phosphate (FAP)–halloysite nanotubes (HNTs) were synthesized with simulated wastewater containing N, P, and Fe pollutants as raw materials. The adsorption–chemical precipitation *in situ* method was used to synthesize the target products, and the optimal conditions for the synthesis of the FAP–HNTs were obtained. Fourier transform Infrared (FTIR) spectroscopy, energy-dispersive spectroscopy (EDS), scanning electron microscopy, transmission electron microscopy, and thermogravimetric analysis were conducted to characterize the samples. The FAP particle size was 20–30 nm in the FAP–HNTs. The FTIR spectra demonstrated that a small amount of water in the FAP–HNTs promoted the curing reaction. The FAP–HNTs and Exolit OP 1230 (OP) were introduced into epoxy (EP) to prepare the polymer nanocomposites. The heat release rate (HRR) and flammability of the EP composites were tested by microscale combustion calorimetry and UL-94 instruments. The mechanical properties of the EP composites also were tested by a tension testing system. The results indicate that the flame retardancy and mechanical properties of the EP composites were improved by FAP–HNT. The addition of FAP–HNT and OP gave rise to an evident reduction of HRR and a prolonged burning time for the EP. EP/FAP–HNT/OP (20) (where 20 is the loading weight percentage) passed the UL 94 V-0 rating. The analysis of the char revealed the synergy of the FAP–HNTs and OP in reducing the flammability of the polymers. We concluded that these polymers show potential for applications in wastewater treatment and N/P recycling. © 2014 Wiley Periodicals, Inc. J. Appl. Polym. Sci. **2015**, *132*, 41681.

KEYWORDS: composites; flame retardance; graphene and fullerenes; mechanical properties; nanotubes

Received 6 May 2014; accepted 23 October 2014

DOI: 10.1002/app.41681

INTRODUCTION

Eutrophication is one of the most serious water pollution problems, and it stems from nitrogen (N) and phosphorus (P) nutrient enrichment of wastewater. So, a number of nutrient-removal processes for N and/or P from wastewaters have been developed. Biological processes,[1] adsorption,[2] and chemical precipitation[3] have been widely used for ammonium nitrogen and phosphate removal from contaminated water. Among these methods, the adsorption benefits from the simplicity of operations and a low operation cost. To further improve the efficiency of the adsorption, ferric oxides[4] and halloysite have attracted attention because of their cost effectiveness, chemical stability over a wide pH range, and environmentally benign properties.[5] Halloysite nanotubes (HNTs)[6] have the chemical structure $Al_2Si_2O_5(OH)_4{\cdot}2H_2O$. Their elemental composition is similar to kaolinite, but they are rolled in tubes with a diameter of 50 nm and a length of about 1000 nm. HNTs exhibit a higher adsorption capacity for both cationic and anionic compounds because they have negative SiO_2 groups on their outer surface and positive Al_2O_3 groups on their inner lumen surface. It is worth noting that adsorbent HNTs are also flame retardant.[7] HNTs have been investigated as an alternative polymer nanofillers for nanotubes (CNTs) and introduced into nylon 6,[8] epoxy (EP),[9] and so on to act as a char-forming additive.[10] These polymer nanocomposites also exhibit remarkable performances, such as reinforced mechanical properties and reduced thermal expansion.[11,12] To enhance the flame retardancy and mechanical properties, the P intercalation of HNTs has been studied further. When polyamide 6 was blended with phenyl phosphonic acid-functionalized HNTs, a synergistic

Table I. Summary of the Nomenclature, Composition, and Test Items of the EP Composites

Nomenclature[a]	Additives and loading (wt %)	Test items
EP/HNT (20)	HNT (20)	TEM, MCC, and tension testing
EP/FAP (20)	FAP (20)	FTIR spectroscopy, TGA, and MCC
EP/OP (5, 10, 15, and 20)	OP (5, 10, 15, and 20)	Tension testing, MCC, and UL-94
EP/FAP/OP (5, 10, and 20)	FAP (2.5, 5, and 10) + OP (2.5, 5, and 10)	TGA and tension testing
EP/FAP/OP (201)	FAP (6.67) + OP (13.33)	TGA
EP/FAP–HNT (5, 10, 15, and 20)	FAP–HNT (5, 10, 15, and 20)	TGA, UL-94, EDS, SEM, and FTIR spectroscopy
EP/FAP–HNT (201)	FAP–HNT (20) (FAP:HNT = 10:1,w/w)	TEM
EP/FAP–HNT/OP (5, 10, 15, 20, and 25)	FAP–HNT (2.5, 5, 7.5, 10, and 12.5) + OP (2.5, 5, 7.5, 10, and 12.5)	MCC, UL-94, EDS, and tension testing

[a] In these composites, the composition of FAP–HNT was FAP/HNT = 1:1 w/w.

fire-retardant system, combustive performance improved significantly.[13]

As for the chemical precipitation method, magnesium ammonium phosphate precipitation methods are effective technologies for wastewater treatment.[14] In addition, the synthesis of ammonium metal phosphates [AMPs; $MNH_4PO_4{\cdot}H_2O$; M = Mn(II), Fe(II), Co(II), Zn(II), or Cu (II)] has been known for a long time.[15,16] Some AMPs have been widely used in industry as pigments and fertilizers. Ferrum ammonium phosphate ($FeNH_4PO_4{\cdot}H_2O$; FAP) also has been introduced to prepare lithium iron phosphate ($LiFePO_4$)[17] or applied as flame retardants.[18] So, the chemical precipitation method shows good prospects in the field of denitrification and P removal. However, on the one hand, except for with magnesium ammonium phosphate, the AMP precipitation method has seldom been used to treat eutrophic water. The synthesis and application conditions of AMPs also need to be optimized further. On the other hand, AMPs with a single function and a low additional value could not be applied widely. So, despite recent progress, a method for preparing and using AMPs properly still needs to be elucidated.

In this study, simulated wastewater from steelworks containing ferrum sulfate was treated in combination with simulated eutrophication wastewater containing a high concentration of ammonium nitrogen and phosphate. First, the ammonium nitrogen and phosphate were adsorbed by the HNTs. Second, multifunctional FAP–HNT nanocomposites were synthesized *in situ* through the addition of ferrum sulfate. Third, to lower the cost and enhance the flame retardancy and mechanical performance of materials, the FAP–HNTs and Exolit OP 1230 (OP) flame retardant were introduced into EP. During processing, the optimum conditions of these processes were determined, and the products were characterized and tested by Fourier transform infrared (FTIR) spectroscopy, scanning electron microscopy (SEM)/energy-dispersive spectroscopy (EDS), thermogravimetric analysis (TGA), transmission electron microscopy (TEM), microscale combustion calorimetry (MCC), UL-94 testing, and a tensile testing system. Finally, on the basis of the previous analysis, the synergy of FAP–HNT and OP 1230 was examined.

EXPERIMENTAL

Materials

Ammonium sulfate [$(NH_4)_2SO_4$], sodium phosphate, tribasic dodecahydrate ($Na_3PO_4{\cdot}12H_2O$, Reagent Plus, >99.0%), and iron(II) sulfate hydrate $FeSO_4{\cdot}7H_2O$ (ACS reagent, >99.0%) were purchased from Sigma-Aldrich Co. LLC. Magnobond 56 Part B (an industrial-grade modified polyamide curing agent) was obtained from Magnolia Plastics, Inc. EPON resin 828 (reaction product: bisphenol A–epichlorohydrin; number-average molecular weight ≤ 700, industrial grade) was provided by Resolution Performance Products, LLC. HNTs [$Al_2Si_2O_5(OH)_{42}H_2O + SiO_2$, 258.16 g/mol, industrial grade) were purchased from READE Advanced Materials Co., LLC, and were typically 40–200 nm in diameter with various lengths from 500 nm to 1.2 μm. The intumescent flame-retardant OP ($[C_4H_{10}PO_2]_3Al$, 390.3 g/mol, P content ≈ 23 wt %, industrial grade) was obtained from Clariant International, Ltd.

Preparation of FAP and FAP–HNT

FAP was prepared with the chemical precipitation method. The typical synthesis procedure was as follows. $(NH_4)_2SO_4$ (2.76 g, 20.91 mmol), $Na_3PO_4{\cdot}12H_2O$ (15.84,41.67 mmol) and 800 mL of distilled water were added to a 1000-mL beaker. The solution was stirred by magnetic stirrers at 1050 rpm. After the chemicals were dissolved completely, $FeSO_4{\cdot}7H_2O$ (18.32, 65.89 mmol) was added to the previous solution in five separate batches until the pH of solution reached about 9–9.5. During the precipitation, an ultrasound was introduced to disperse the $FeNH_4PO_4$ as prepared. The precipitation reaction proceeded for 30 min at room temperature. The wet products were vacuum-dried at 130°C for 12 h. Finally, the $FeNH_4PO_4$ (8.38 g, yield = 99.2%) was obtained.

The adsorption–precipitation (*in situ*) method was used to prepare the FAP–HNTs. The typical synthesis procedure was as follows. First, $(NH_4)_2SO_4$ (0.69 g) and $Na_3PO_4{\cdot}12H_2O$ (3.69 g) in an aqueous solution were adsorbed by the HNTs (2.00 g) for about 20 min to prepare the PO_4^{3-}—NH_4^+—HNT. Then, the $FeSO_4{\cdot}7H_2O$ (4.28 g) was added to the previous suspension in batches until the pH of solution reached about 9–9.5. During

the precipitation, an ultrasound was introduced to disperse the FAP–HNTs as prepared:

$$HNT + Na_3PO_4{\cdot}12H_2O + (NH_4)_2SO_4 \rightarrow PO_4^{3-}{-}NH_4^{+}{-}HNT \quad (1)$$

$$PO_4^{3-}{-}NH_4^{+}{-}HNT + Fe^{2+} + 12H_2O \rightarrow FeNH_4PO_4 \cdot 12H_2O{-}HNT \quad (2)$$

The wet products were vacuum-dried at 130°C for 12 h. Finally, the FAP/HNTs (4.46 g, yield = 98.3%) were obtained. We also prepared FAP/HNTs containing different concentrations of FAP and HNTs. These FAP/HNTs were used to prepare the EP composites.

Preparation of the EP Composites

To study and compare the flame retardancy and mechanical properties, the neat EPON resin and EP composites containing the following were prepared: (1) 20 wt % HNTs; (2) 20 wt % FAP; (3) 5, 10, 15, and 20 wt % OP; (4) 5, 10, and 20 wt % FAP/OP (FAP/OP = 1:1 w/w); (5) 5, 10, 15, and 20 wt % FAP–HNTs (FAP/HNTs = 1:1–10:1 w/w); and (6) 5, 10, 15, 20, and 25 wt % FAP–HNT/OP (FAP–HNT/OP = 1:1 w/w). The summary of the nomenclature, composition, and test items are listed in Table I.

Both the FAP and FAP–HNT nanoparticles were immersed in EP resin overnight without any disturbance so that the resin could wet the nanoparticles completely. OP was directly mixed with the EP resin or EP resin/FAP–HNT. Then, the solution was treated by ultrasound dispersion for 1 h. All of the procedures were carried out at room temperature. The polyamide curing agent Magnobond 56 PART B was added to the previous EP resin/FAP–HNT nanosuspensions with an EP resin/curing agent at a weight ratio of 100/80 after the sonic dispersion for about 1 h until the viscosity of the solution increased. This was essential for removing the bubbles and for preventing the sedimentation of the FAP–HNT nanoparticles during the curing process. When the viscosity increased to a certain extent, the solutions were poured into silicone molds and cured at room temperature for 24 h. Then, the samples were cured for 3 h at 120°C. After they were allowed to cool down to room temperature naturally, the specimens were obtained.

Characterization and Measurement

FTIR spectroscopy of the samples was performed with an Infinity Gold FTIR instrument (Thermo Mattson) with a liquid-nitrogen-cooled narrow band mercury cadmium tellurium (MCT) (700–4800 cm^{-1}) and a room-temperature deuterated triglycine sulphate (DTGS) detector (400–4800 cm^{-1}). The signal resolution of the FTIR instrument was 1 cm^{-1}, and a minimum of four scans was obtained and averaged within the range 400–4000 cm^{-1}. The FAP and FAP–HNT powders were blended with KBr, and then, the transmittance of the thin KBr disc was tested by FTIR spectroscopy. The EP, EP/FAP, and EP/FAP–HNT films were directly tested by FTIR spectroscopy in absorbance mode.

The morphological changes of the EP/FAP–HNT composite before and after the UL-94 test were examined by SEM (S-5500 instrument) at an accelerating voltage of 20 kV. The associated elemental composition was determined by energy-dispersive analysis by an X-ray (EDAX) facility.

The dispersion of the FAP–HNTs in EP was obtained at 200 kV with a JEOL 2010F TEM instrument. The materials were tested as received with no additional conditioning before testing.

TGA on the EP/FAP–HNT composites (ca. 8.0 mg) were characterized on a Shimadzu TGA-50H instrument in flowing air at 10°C/min from room temperature to 800°C.

MCC was used to characterize the HNT, FAP, FAP–HNTs, and their EP composites with respect to their potential flammability performance. MCC is a method for measuring the heat release rate (HRR) of milligram-sized samples. The rate at which heat is released by a burning material is the single most important parameter determining its hazard in a fire. MCC provides a continuous, direct measurement of the heating value with a very fast response time. In this study, MCC was conducted on 4 ± 1 mg samples with a Govmark microscale combustion calorimeter (model MCC-2) operated at a heating rate of 1°C/s to 750°C in the pyrolysis zone. The samples were tested according to ASTM guidelines (ASTM D 7309−07).[19] The combustion zone was set at 900°C, and the oxygen flow rate was set at 19 mL/min. The HRR in watts per gram of sample was calculated from the oxygen depletion measurements. We obtained the char yield was obtained by weighing the sample before and after the test. The reported values are the averages of three measurements on each compound with a deviation of ±5%.

The mechanical properties of the EP nanocomposites were evaluated with an Instron model 3345 tension testing system in accordance with ASTM D 638 for plastics.[20] The load–displacement curve was obtained, and the ultimate tensile stress (UTS) and elongation at break were calculated accordingly. The average values are reported on the basis of five samples that were tested for each formulation. The specimens were conditioned at 50% relative humidity for 48 h before testing. The testing rate was 10 mm/min, and the environmental temperature was 23°C.

UL-94, a standard, small-scale flame test for the flammability of plastic materials, determines a material's tendency to either self-extinguish or spread its flame once the specimen has been ignited. The ratings for UL-94 range from V-2 to V-0. V-0 is the best rating for a polymer that self-extinguishes and also one that does not drip flaming fragments. The materials were tested as received with no additional conditioning before testing. Five specimens for each formulation were tested.

RESULTS

Preparation and Characterization of the FAP–HNT and EP/FAP–HNT Composites

The FAP and FAP–HNTs were synthesized by chemical precipitation (*in situ* synthesis) methods. For dosages of the $(NH_4)_2SO_4$, $Na_3PO_4{\cdot}12H_2O$, $FeSO_4{\cdot}7H_2O$, and HNTs of 0.69, 3.69, 4.28, and 2.00 g, respectively, the elemental contents (atom %) in the FAP–HNT were as follows: O (61.19), P (4.73), N (9.27), Fe (6.38), Al (8.55), and Si (7.12). As shown in the results, the N content (9.27 atom %; P/N/Fe = 1:1.96:1.35) was higher than the calculated value from the FAP/HNT formula

Table II. Effect of the HNT Concentration on the Yield of FAP–HNT

HNT (mmol/L)	60	38.5	19.5	9.5	1.9
FAP yield (%)	98.2	98.6	99.0	99.4	99.6
FAP–HNT yield (%)	95.7	96.5	99.3	99.8	99.8

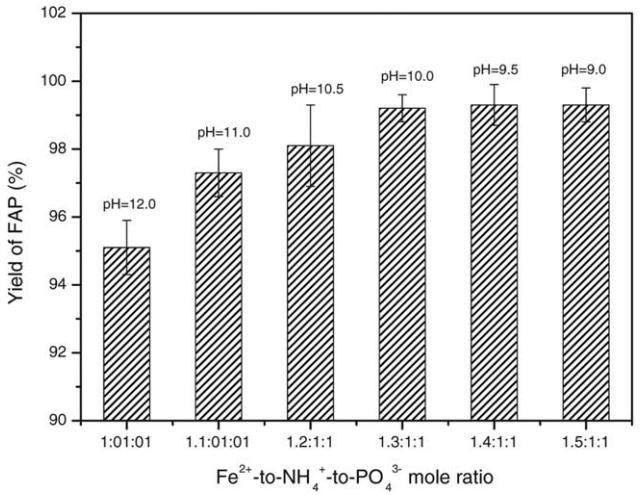

Figure 1. Effect of the Fe^{2+}-to-NH_4^+-PO_4^{3-} molar ratio on the yield of FAP.

(P/N/Fe = 1:1:1). This was due to the adsorption of some ammonium on the surface of the product. These FAP–HNTs (FAP/HNT = 1:1 w/w) were used to prepare the EP composite specimens.

Furthermore, the effects of the reaction time, reaction temperature, pH, and ratio of raw materials on the yield and composition of the FAP and FAP–HNTs were studied. The effects of the HNT concentration on the yields of FAP and FAP–HNTs are shown in Table II. Because the concentrations of $FeSO_4{\cdot}7H_2O$, $(NH_4)_2SO_4$, and $Na_3PO_4{\cdot}12H_2O$ were 0.05, 0.027, and 0.05 mol/L, respectively, FAP yielded increases from 98.2 to 99.6%, and the FAP–HNTs yielded increases from 95.7 to 99.8% when the HNT concentration decreased

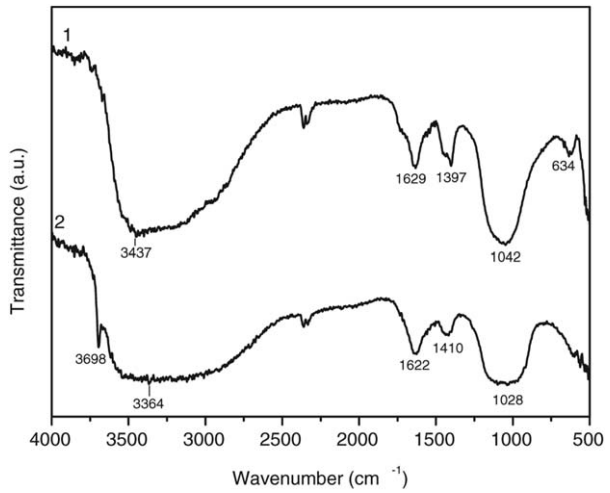

Figure 2. FTIR spectra of (1) FAP and (2) FAP–HNT.

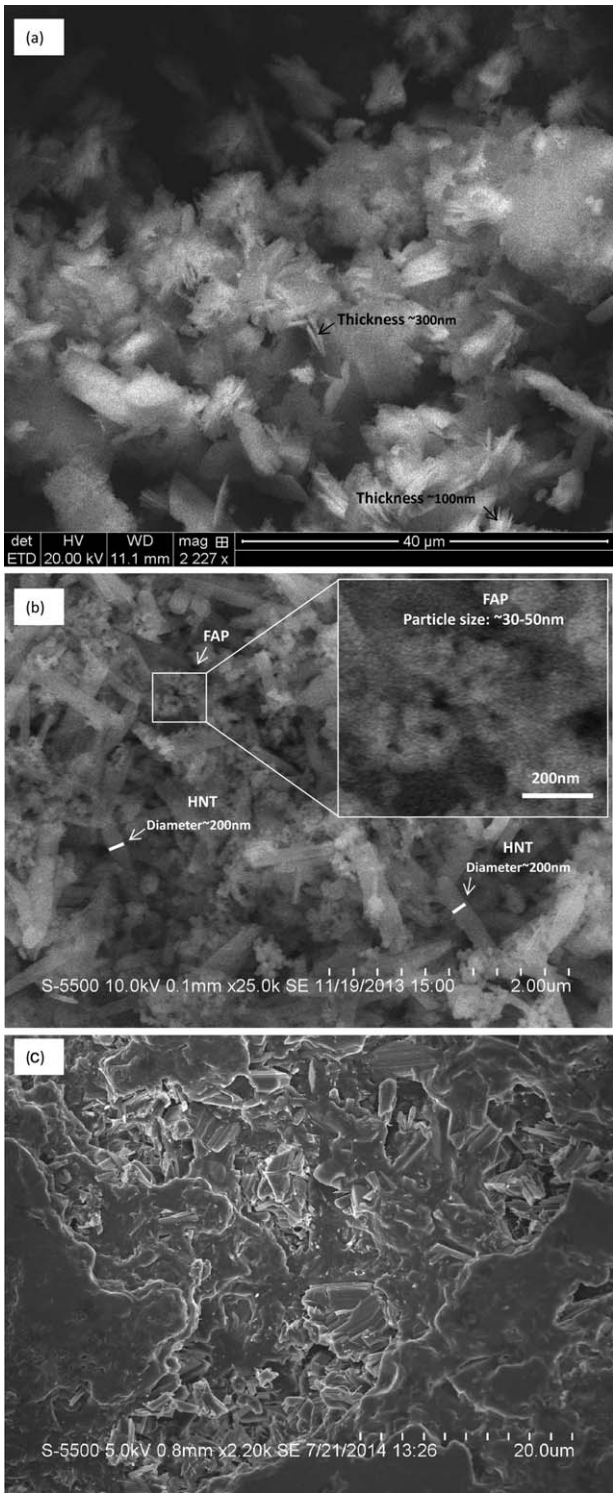

Figure 3. SEM images of the (a) FAP (synthesis without ultrasound), (b) FAP–HNT (ultrasound-assisted synthesis), and (c) EP/FAP–HNT/OP (20) nanocomposites. The insets in parts b and c show the SEM images of the neat FAP and OP, respectively.

from 60 to 1.9 mmol/L. This may have been due to the effect of the HNTs on the crystallization of FAP. It is worth noting that there was still some adsorbed water in the products that was difficult to remove because of the strong

Table III. Effect of the $Fe^{2+}/NH_4^+/PO_4^{3-}$ Molar Ratio on the Composition of FAP–HNT (atom %)

Nomenclature	$Fe^{2+}/NH_4^+/PO_4^{3-}$	C	O	P	N	Fe	Al	Si
FAP-HNT-1	1.4:1:1	1.14	61.19	4.73	9.27	6.38	8.55	7.12
FAP-HNT-2	1.3:1:1	1.13	60.28	3.96	8.96	4.74	10.19	9.74
FAP-HNT-3	1.2:1:1	1.16	61.31	3.46	8.88	4.17	10.63	9.73
FAP-HNT-4	1:1:1	0.99	61.45	3.11	8.94	3.13	11.30	10.48

polarity of FAP and the high adsorption capacity of the HNTs. So, the real yield of the FAP–HNTs should have been less than the experimental value.

As shown in Figure 1, when the $Fe^{2+}/NH_4^+/PO_4^{3-}$ molar ratio varied from 1:1:1 to 1.5:1:1, that is, with increasing Fe^{2+} dosage, the FAP yield increased from 95.1 to 99.3%, with the pH of the solution decreasing from 12 to 9.5. This indicated that the Fe^{2+} reacted with NH_4 and PO_4^{3-} adequately. On the basis of the previous analysis, the optimal conditions for the synthesis of the FAP–HNTs were as follows: a reaction time of about 30–40 min, a reaction temperature from room temperature to 80°C, a pH of about 9.5, an $Fe^{2+}/NH_4^+/PO_4^{3-}$ molar ratio of 1.4:1:1, and an HNT concentration of 1.9–19.5 mmol/L; some these values were in accordance with the literature.[21]

The FTIR spectra of the samples are shown in Figure 2. The marked peaks of FAP [Figure 2(1)] were located at 3698 cm^{-1} (OH^-), 3437 cm^{-1} (ν_{H-O-H}), 1629 cm^{-1} (β_{P-O}, ν_{P-O}), 1397 cm^{-1}(ν_{P-O-N}), 1042 cm^{-1} (as_{P-O-N}), and 634 cm^{-1}(β_{P-O}). The charateristic adsorption bands of the FAP–HNTs [Figure 2(2)] were similar to those of FAP. There was a strong and wide O—H adsorption band (3364 cm^{-1}) in the FAP–HNTs; this indicated some constructive and adsorbed water in the FAP–HNTs. The water was difficult to remove completely.[22]

Typical morphologies of the FAP, FAP–HNTs, and EP/FAP–HNT/OP (20) nanocomposites are shown in Figure 3. Figure 3(a) shows the FAP slices prepared without ultrasound. The thickness of the FAP slices ranged from 100 to 300 nm. The FAP slices aggregated together to form clusters. In comparison with the FAP, the FAP–HNTs prepared by *in situ* synthesis with an ultrasound-assisted method showed uniform dispersion [Figure 3(b)]. The diameter of the HNTs was about 200 nm, and that of the FAP particles was about 20–30 nm, although some FAP particles aggregated together incompactly. Generally, the nucleation, particle growth, and crystallization rates increase as a result of the application of ultrasound.[23] In this study as well, a highly crystalline FAP with a smaller average particle diameter was obtained at shorter synthesis times; this resulted from the application of ultrasound and the HNTs. The ultrasound provided a mechanical disturbance to increase the crystallization rate and disperse the crystals. The HNTs also acted as a disperser to lower the average crystal size of FAP. Figure 3(c) presents an SEM image of the EP/FAP–HNT/OP (20) nanocomposites. Compared to the neat OP [inset of Figure 3(c)], the OP was dispersed uniformly in EP. Some HNT nanorods were also found in the composites, although they were very small.

To determine the effect of the $Fe^{2+}/NH_4^+/PO_4^{3-}$ molar ratio on the composition of the FAP–HNTs, the concentration of HNTs was held at 20 mmol/L while the $Fe^{2+}/NH_4^+/PO_4^{3-}$ molar ratio varied from 1.4:1:1 to 1:1:1 ($C_{NH4} = 6$ mmol/L). Examination by SEM/EDS of the FAP–HNTs (Table III) showed that as the $Fe^{2+}/NH_4^+/PO_4^{3-}$ molar ratio increased from 1:1:1 to 1.4:1:1, the Fe, N, and P relative content in the composites increased from 3.13 to 6.38, 8.88 to 9.27, and 3.11 to 4.37 atom %, respectively; this indicated the simultaneous increasing percentage conversion and yield of the FAP–HNTs. It is worth noting that in our experiment, we did not use additional acid to neutralize the solution containing N and P. As we know, the $(NH_4)_2SO_4$ and $Na_3PO_4{\cdot}12H_2O$ were both Lewis bases, whereas the $FeSO_4{\cdot}7H_2O$ was a Lewis acid. So, neutralization was easy in this study. The excess Fe^{2+} could be recycled or removed by the oxidation and precipitation method.

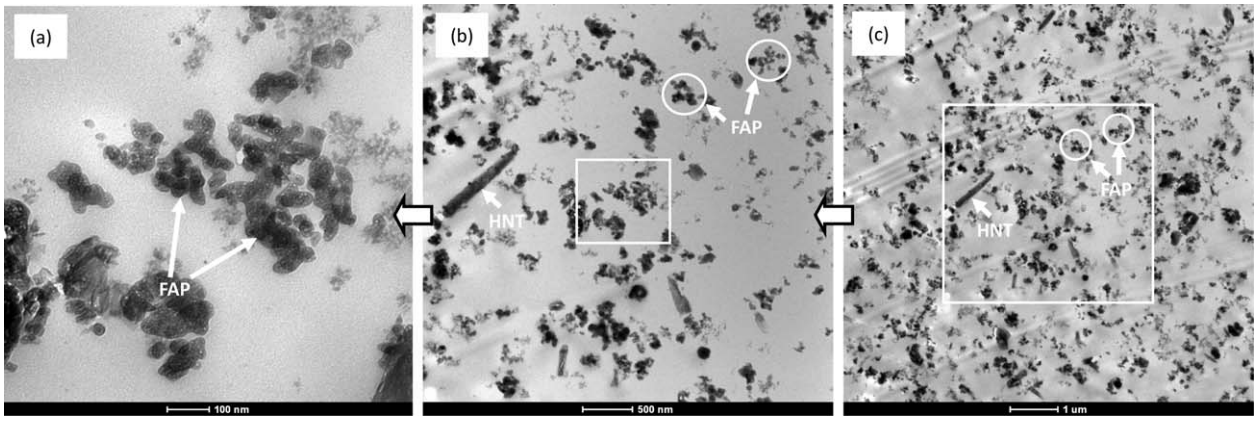

Figure 4. TEM images of the EP/FAP–HNT (201) at different magnifications.

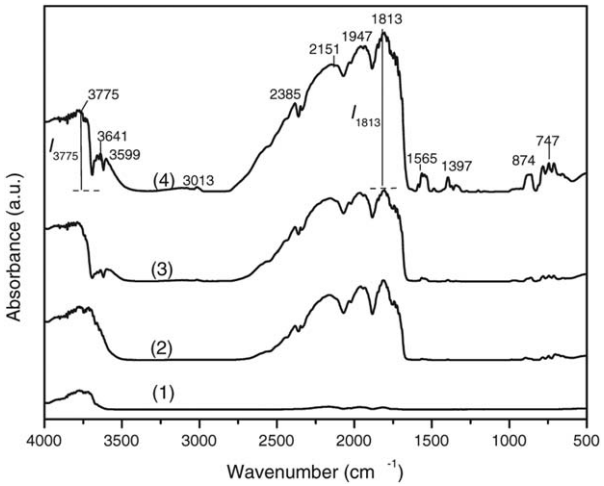

Figure 5. FTIR spectra of (1) EP, (2) EP/FAP (20), (3) EP/FAP–HNT (5), and (4) EP/FAP–HNT (15).

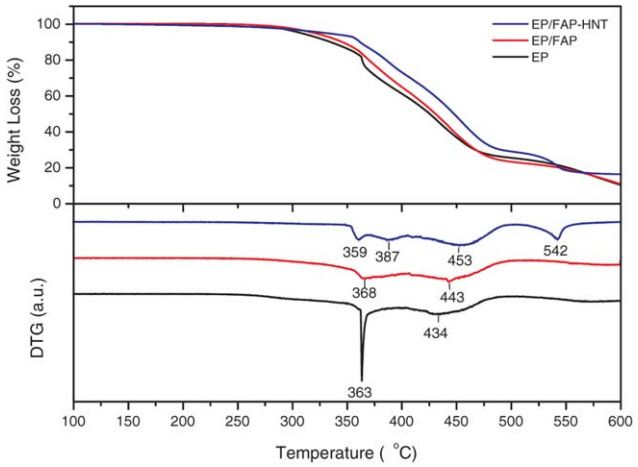

Figure 7. TGA and DTG curves of EP, EP/FAP (20), and EP/FAP–HNT (20). [Color figure can be viewed in the online issue, which is available at wileyonlinelibrary.com.]

Figure 4 shows the TEM photos of the EP/FAP–HNT polymer nanocomposites. It can be seen that the FAP–HNTs were dispersed in the matrix very uniformly. FAPs always tend to aggregate with each other, so it is difficult to disperse them homogeneously in polymers. However, the dispersion of FAPs in the FAP–HNTs was better than that of the neat FAPs because of the dispersal of HNTs. Individually separated HNTs with lengths of 100–1000 nm and a diameter of 50–150 nm were found in the samples. The strong interfacial bonding between the matrix and FAP–HNTs led to potentially good mechanical properties of the EP/FAP–HNT polymer nanocomposites.

To verify the interfacial reactions between the FAP–HNTs and EP matrix, FTIR experiments were conducted on the composites. The hydroxyl was the main reactive group on the FAP–HNTs. The surfaces of the HNTs were curved or rolled. The interfacial reactions between the HNTs and the matrix were mainly interactions between aluminols, silanols, EP groups, and hydroxyl groups. The FTIR adsorption spectrum of the cured EP is shown in Figure 5(1). The characteristic peaks of EP were located at 2151, 1947, and 1813 cm^{-1}. These peaks also existed in the EP/FAP [Figure 5(2)] and EP/FAP–HNTs [Figure 5(3,4)]. In comparison with EP, the marked peaks of EP/FAP were located at 2385, 1565, 1397, 874, and 747 cm^{-1}. As for the EP/FAP–HNTs, the new absorptions around 3599 and 3641 cm^{-1} were attributed to Al—OH stretching in the HNTs. A similar shoulder peak (~3633 cm^{-1}) of Fe—OH in EP/FAP was observed. There was no marked peak of amino groups (~3343 cm^{-1}). This was due not only to the release of NH_3 during heating and processing but also to the low loading of the FAP–HNTs. The absorptions around 3775 cm^{-1} for all of the samples were attributed to the O—H stretching of the free water. Noticeably, the intensity ratio of $I_{3775\ cm-1}/I_{1813\ cm-1}$ decreased from 110% (EP) to 51% [EP/FAP–HNT (15)], in which $I_{1813\ cm-1}$ is the intensity of the C—H vibrations of EP. Choi *et al.*[24] reported the effect of water addition on the curing kinetics of an EP–amine thermoset. The FTIR spectra demonstrated that a small amount of water addition significantly accelerated the curing reaction in terms of epoxide conversion, with water acting as a catalyst for the reaction. The decreasing

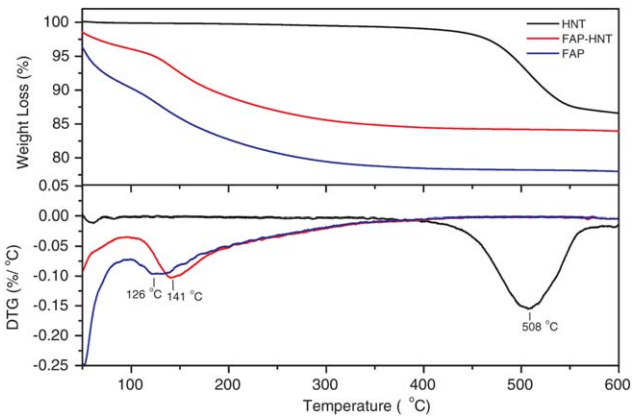

Figure 6. TGA and DTG curves of FAP, HNT, and FAP–HNT. [Color figure can be viewed in the online issue, which is available at wileyonlinelibrary.com.]

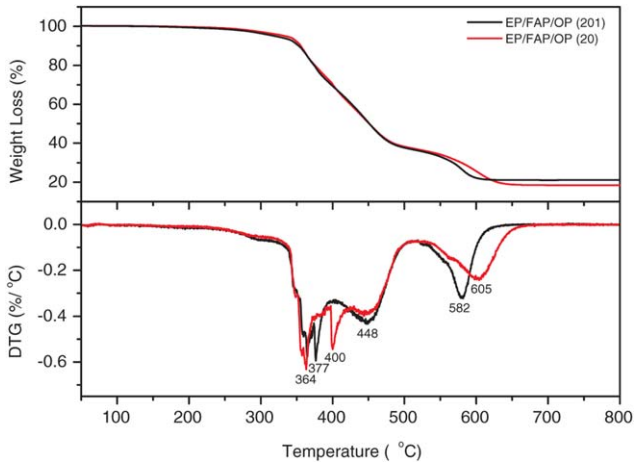

Figure 8. (a) TGA and (b) DTG curves of EP/FAP/OP (20) and EP/FAP/OP (201). [Color figure can be viewed in the online issue, which is available at wileyonlinelibrary.com.]

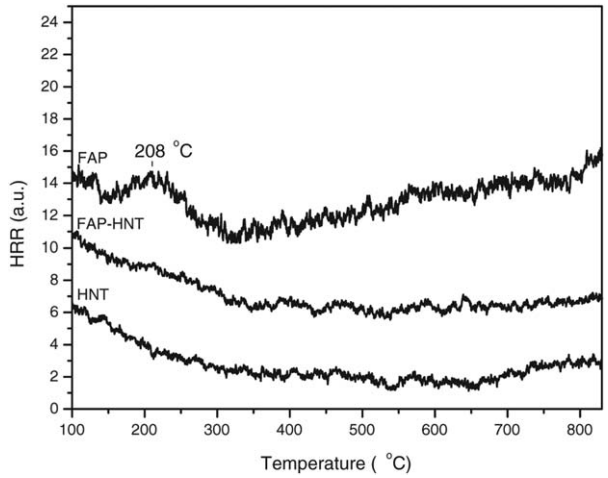

Figure 9. HRR curves of HNT, FAP, and FAP–HNT.

intensity ratio of $I_{3775\ cm-1}/I_{1813\ cm-1}$ in this study also confirmed the reaction between water and EP. Similarly, compared to EP/FAP (20), the intensity ratio of $I_{3641\ cm-1}/I_{1813\ cm-1}$ of EP/FAP–HNT (5) decreased from 45 to 14%. We, therefore, concluded that the aluminols may have reacted with the EP groups; that is, the curing of EP was accelerated by the FAP–HNTs.[25] However, as the loading of the FAP–HNT increased from 5 to 15 wt %, the intensity ratio of $I_{3641\ cm-1}/I_{1813\ cm-1}$ increased from 14 to 23%; this indicated a negative effect of too much water on the curing reaction between the aluminols and the EP groups.

Thermal Properties

The TGA and derivative thermogravimetry (DTG) curves of the HNTs are shown in Figure 6. For the as-received halloysite particles, a weight loss of around 13.5% occurred after the temperature exceeded 600°C; this represented the removal of the interlayer water. In the DTG curve, there was an endothermic signal with the maximum at 508°C; this indicated the dehydration of the particles with basal spacing during moderate heating.

Table IV. Summary of the HRR Reduction and PBT of the EP Composites in Comparison with the EP

	HRR reduction (%)		PBT (s)	
Specimen	First peak	Second peak	First peak	Second peak
EP/FAP (20)	41	26	4	29
EP/FAP–HNT (20)	33	26	1	29
EP/FAP–HNT/OP (20)	39	37	20	55

During decomposition, the composition of the HNTs changed from $Al_2Si_2O_5(OH)_4{\cdot}2H_2O$ to metahalloysite $[Al_2Si_2O_5(OH)_4]$ over 200°C. Finally, $Al_2S_2O_5$ was obtained at about 600°C. The bibliographic data show that upon heating between room temperature and at about 600°C, the $NH_4FePO_4{\cdot}H_2O$ decomposed according to a two-stage process. The first stage was attributed to the loss of crystallized water, whereas the second was related to the loss of structural water and ammonia. The decomposition product of FAP in N was $Fe_2P_2O_7$. In this study, FAP had a final residue of 78.0% at 600°C in an air atmosphere. In the DTG curve, a weight loss signal with a maximum at 126°C was observed. Beatriz *et al.*[26] reported that during the thermogravimetry (TG) of FAP in an O_2 atmosphere, the endothermic desorption process was coupled with an Fe(II)→Fe(III) oxidation. The evacuation of water and ammonia from FAP occurred above 126°C. The TG/DTG curves of the FAP–HNTs were obtained in an air atmosphere. These TG curves consisted of two continuous stage mass loss processes. The total mass loss up to 600°C was 16.1%. The DTG curve showed a minimum (−0.10%/°C) at 141°C, probably as a consequence of the $NH_4FePO_4{\cdot}H_2O$ nanoplate thermal decomposition.[27] The results indicate the process of the loss of water and ammonia.

As shown in the TG/DTG curves of the EP, EP/FAP, and EP/FAP–HNTs (Figure 7), there were two stages of weight loss in EP at 363 and 434°C, respectively. As for EP/FAP, similar peaks

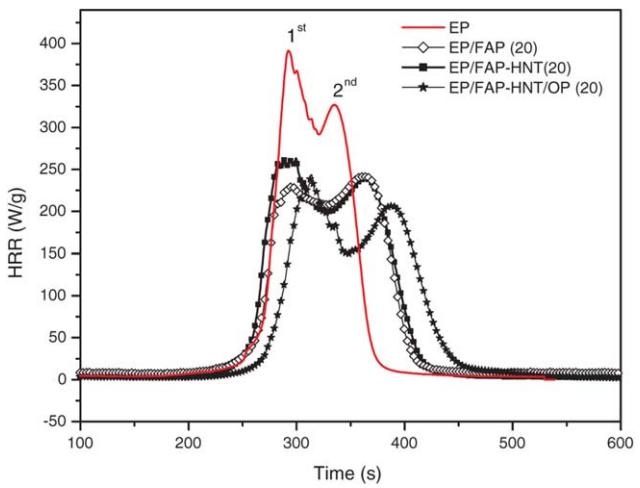

Figure 10. HRR curves of EP/HNT (20), EP/FAP (20), and EP/FAP–HNT/OP (20). [Color figure can be viewed in the online issue, which is available at wileyonlinelibrary.com.]

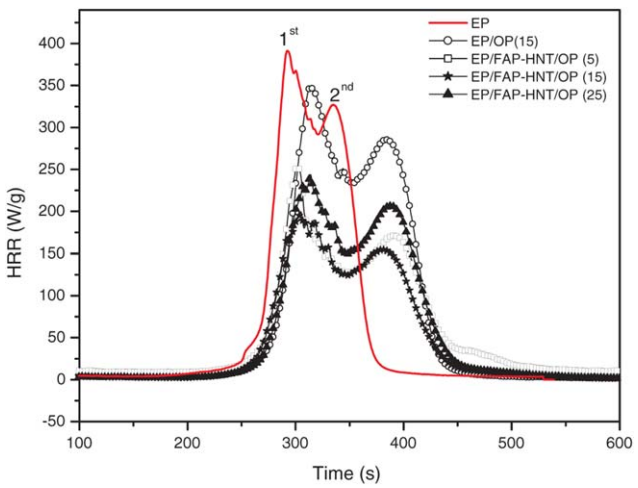

Figure 11. HRR curves of EP, EP/OP (15), and EP/FAP–HNT/OPs. [Color figure can be viewed in the online issue, which is available at wileyonlinelibrary.com.]

Table V. Summary of the HRR Reduction and PBT of the EP Composites in Comparison with the EP

	HRR reduction (%)		PBT (s)	
Specimen	First peak	Second peak	First peak	Second peak
EP/OP (15)	11	13	22	49
EP/FAP–HNT/OP (5)	36	47	9	58
EP/FAP–HNT/OP (15)	51	53	14	46
EP/FAP–HNT/OP (20)	39	37	20	55
EP/FAP–HNT/OP (25)	38	36	22	52

moved to 368 and 443°C; this indicated that the EP/FAP was more stable than EP. In the EP/FAP–HNT curve, there were four peaks at 359, 387, 453, and 542°C; these resulted from the decomposition of EP, FAP, and HNTs.

The TGA and DTG curves of EP/FAP/OP with different FAP/OP weight ratios are shown in Figure 8. The weight of residue of EP/FAP/OP (20) (FAP/OP = 1:1) was 18.04%; this was lower than that of EP/FAP/OP (201) (20.88%). As shown in the DTG curves, there were two stages of weight loss. In the first stage, the EP/FAP/OP (20) lost weight at 364, 400, and 448°C; this was different from EP/FAP/OP (201) (with weight losses at 364, 377, and 448°C). In the second stage, EP/FAP/OP (20) (605°C) showed more stable properties than EP/FAP/OP (201) (582°C). Gracik and Long[28] reported the relationship between the amount of TG char measured at various sample degradation temperatures and the limiting oxygen index (LOI) at elevated sample temperatures. Analysis of the experimental results indicated that the amount of TG char was directly proportional to the LOI value of most of the thermoplastics evaluated. The higher the amount of TG char of a thermoplastic material was, the higher its LOI value was; that is, it had a lower flammability.

Flammability

MCC was introduced to characterize the HNTs, FAP, FAP–HNTs, and their EP composites with respect to their potential flammability performance. The rate at which heat is released by a burning material is the single most important parameter determining its hazard in a fire, particularly in an enclosed space. MCC focuses on a quantitative analytical test that correlates the fire behavior or flame test performance with the material properties. Figure 9 presents the HRR curves of the HNTs, FAP, and FAP–HNTs. A marked peak at 208°C for FAP was observed; this indicated the decomposition of FAP. There was no marked peak for the HNTs and FAP–HNTs because of the small amount of FAP in the HNTs. By comparison with the TGA/DTG curve of FAP (Figure 6), during combustion, water and ammonia were released from both the FAP and HNTs. Simultaneously, the composition of the HNTs changed from $Al_2Si_2O_5(OH)_4{\cdot}2H_2O$ to metahalloysite $[Al_2Si_2O_5(OH)_4]$ over 200°C. Generally, the decomposition temperature of halogen-free flame retardants should be close to or lower than that of polymers. So, the formula of the EP composites could be optimized on the basis of the HRR, heat releasing time, and decomposition temperature of the flame retardants.[29]

Figure 10 presents the HRR curves of the pure EP and EP composites. The HRR reduction and prolonged burning time (PBT) in comparison with EP are summarized in Table IV. The results show that the addition of FAP, FAP–HNT, and FAP–HNT/OP (20) gave rise to 41, 33, and 39% reductions in HRR at the first peak and 26, 26, and 37% reductions at the second peak, respectively, compared to that of neat EP. Also, a PBT of the EP composites was observed. EP/FAP–HNT/OP (20) showed the maximum PBT (~55 s at the second peak); this indicated a good flame retardancy of FAP–HNT/OP.

Furthermore, the effect of the loading of FAP/OP on the HRR of EP/FAP/OP was studied. As shown in Figure 11, through the addition of the FAP–HNTs and OP to EP, the HRR of the EP composites decreased substantially. The HRR reduction and PBT of EP composites compared to those of the neat EP are summarized in Table V. The results indicate that as the FAP–HNT/OP loading increased from 5 to 15 wt %, the HRR of EP/FAP–HNT/OP decreased sharply, and EP/FAP–HNT/OP (15) exhibited a 51–53% reduction in HRR and a 14–46 PBT compared to that of neat EP. However, as the FAP–HNT/OP loading increased to 20 and 25 wt

Table VI. Summary of the UL-94 Flammability Tests of the EP and EP Nanocomposites

Specimens	UL-94 rating	t_1 (s)	t_2 (s)	t_3 (s)	Burnt to clamp	Dripping	Cotton ignition
Neat EP	Failed	16.2	3.4	6.6	Yes	Yes	Yes
EP/FAP–HNT (5)	Failed	48.2	N/A	N/A	Yes	Yes	Yes
EP/FAP–HNT (10)	Failed	42.0	N/A	N/A	Yes	Yes	Yes
EP/FAP–HNT (15)	Failed	29.7	N/A	N/A	No	No	No
EP/FAP–HNT (20)	V-2	24.7	6.5	N/A	No	No	No
EP/OP (15)	V-0	7.7	5.3	0	No	No	No
EP/FAP–HNT/OP (10)	V-2	24.5	12.2	3.2	No	Yes	Yes
EP/FAP–HNT/OP (15)	V-1	22.0	9.4	0	No	No	No
EP/FAP–HNT/OP (20)	V-0	7.4	4.0	0	No	No	No
EP/FAP–HNT/OP (25)	V-0	3.8	3.1	0	No	No	No

N/A, not applicable; t_1, t_2, and t_3 are the average values of five specimens.
t_1, afterflame time after first flame application; t_2, afterflame time after second flame application; t_3, afterglow time after second flame application.

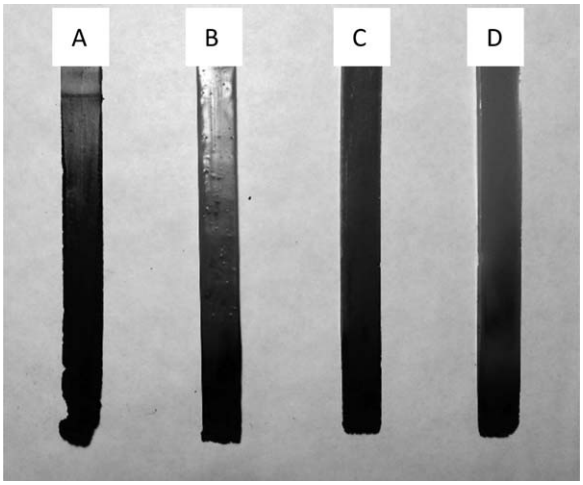

Figure 12. Specimens after UL-94 testing: (A) EP/FAP–HNT/OP (5), (B) EP/FAP–HNT/OP (15), (C) EP/FAP–HNT/OP (20), and (D) EP/FAP–HNT/OP (25).

%, there was no obvious improvement in HRR, except for the increase in the PBT from 22 to 55 s. In comparison with EP/OP (15), EP/FAP–HNT/OP (15) showed a better HRR reduction and a similar PBT; this indicated a good flame retardancy. The mechanism of FAP–HNT/OP in reducing the flammability of the polymers was probably due to the synergistic effect of the FAP–HNTs and OP. A barrier effect on the surface of the polymers created by the FAP–HNTs and OP could have slowed down the heat and mass transfer between the gas and condensed phases and shielded the underlying material from further combustion.[30,31]

The flammability properties of polymer nanocomposites are commonly assessed with UL 94 tests.[32] On the basis of the peak HRR results, we expected that an increase in the UL 94 rating would occur with increasing additive loading. The UL-94 flammability test results of the EP and EP nanocomposites are summarized in Table VI. They show that the neat EP failed to pass the UL 94 rating, whereas EP/OP (15) passed the UL 94 V-0 rating. The EP/FAP–HNT composites containing 5–20 wt % FAP–HNTs failed to pass the UL 94 V-0 rating, but the dripping was improved by the addition of 15–20 wt % FAP–HNTs. Compared to the EP/FAP–HNTs, the EP/FAP–HNT/OP composites exhibited better flame-retardancy properties. EP/FAP–HNT/OP (20) and EP/FAP–HNT/OP (25) pass the UL 94 V-0 rating. The flame retardancy of the EP composites was enhanced obviously with increasing FAP–HNT/OP loading from 10 to 25 wt %.

Further evaluation of the t_1 and t_2 results suggested that the concentration of FAP–HNT/OP affected the ability of the composite to sustain ignition. EP/FAP–HNTs or EP/FAP–HNT/OP

Table VII. Elemental Composition (wt %) of the Residue After UL-94 Testing

Specimen	P	C	O	Fe	Al	Si
EP/FAP-HNT/OP (20)	3.4	13.1	43.4	11.7	3.3	25.1
EP/FAP-HNT (20)	3.3	11.8	48.0	11.4	1.9	23.6

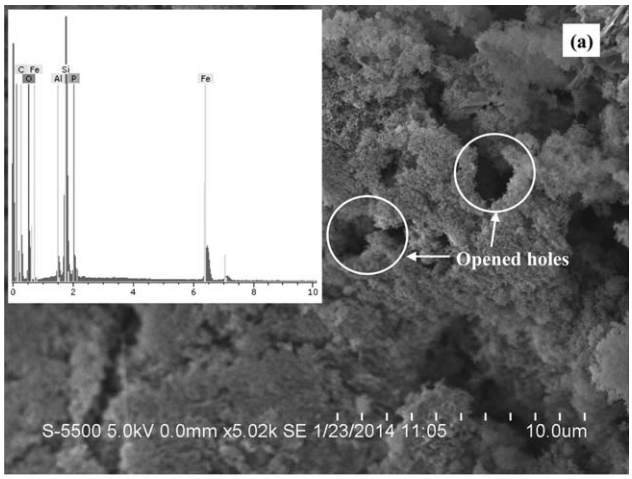

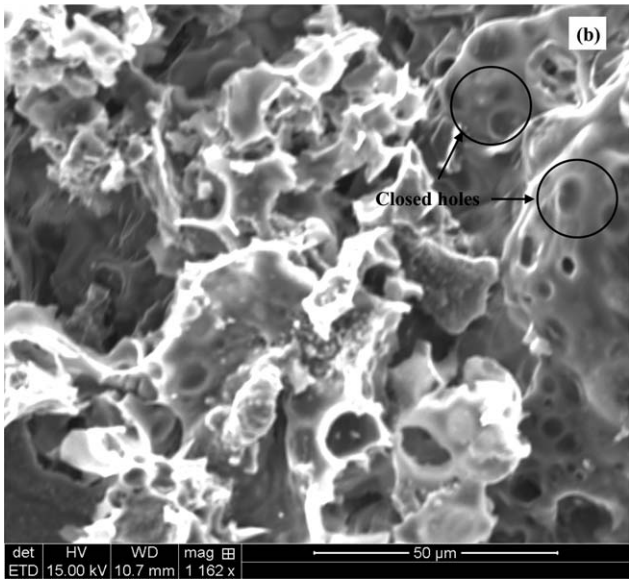

Figure 13. SEM images of (a) EP/FAP–HNT (20) and (b) EP/FAP–HNT/OP (20) after UL–94 testing. The inset indicates the EDS result of char.

with less than 10 wt % additives ignited after the first 10 s of exposure to flame (t_1), whereas the composites with FAP–HNT/OP concentrations of greater than 10 wt % failed to ignite. Cogen *et al.*[33] reported that the mineral fillers could reduce HRR below the threshold value through decreases in the flaming combustion efficiency and fuel content.

A further possible explanation for these observations could have been that during exposure to the flame, FAP decomposed, and the residue/HNTs migrated to the surface as the polymer melted and acted as a heat shield by forming an inert mineral/char layer between the source of the heat and the polymer; this inhibited the release of volatile gases for subsequent ignition.[34]

Figure 12 illustrates the effects of the flammability tests on the EP nanocomposites with various loadings of FAP–HNT/OP. Dripping was observed in the EP/FAP–HNT/OP (5) specimen, and also, the sample was seriously damaged. None of the EP nanocomposites exhibited dripping when the FAP–HNT/OP loading reached 15, 20, or 25 wt %, respectively. Higher FAP–HNT/OP loadings

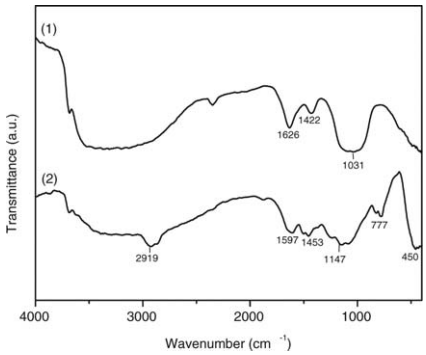

Figure 14. FTIR spectra of (1) FAP–HNT and (2) char of EP/FAP–HNT (20).

increased the samples' resistance to the flame, as shown from their appearance along the specimens. Rigid char without expansion was observed in all of the specimens. So, the condensed-phase, flame-retarding mechanism played a key role in the fire resistance.

Analysis of the Char

To determine the flame-retarding mechanism, the char formed after UL 94 testing was tested by means of SEM/EDS and FTIR spectroscopy. Table VII illustrates the elemental composition of the residue. The EDS results indicated a loss of N, O, and P shown by the change in the N/O/P count ratios in comparison with Table II. This was partly due to dehydration, decomposition, and subsequent dehydroxylation, which was previously shown by TGA. It is known that a higher carbon content and lower oxygen content indicate better char-forming performance or antioxidation degree of the char. In comparison with that of EP/FAP–HNT (20) (11.8 atom %), the carbon content of EP/FAP–HNT/OP (20) (13.1 wt %) was higher. However, the oxygen content of the EP/FAP–HNT/OP (20) (43.4 wt %) was lower than that of EP/FAP–HNT (20) (48.0 wt %); this indicated better char-forming performance for FAP–HNT/OP. This was attributable to the synergistic effect of the FAP-HNTs and OP.

Figure 13 presents the SEM images of EP/FAP–HNT (20) and (b) EP/FAP–HNT/OP (20) after UL-94 testing. The inset [Figure 13(a)] shows the EDS results of the char (data shown in Table VII). The outer surface of the char seemed fluffy and in status lacunaris. Most of the holes in the EP/FAP–HNT (20) char were opened. In comparison, most of the holes in EP/FAP–HNT/OP (20) were closed. Because the swollen inner structure provided a good barrier to the transfer of heat, mass, and flammable gases during combustion, the char with closed holes was better than that with open holes. These closed holes depended on the melt viscosity of the composites, gas source, and releasing time of the flame retardants, the stability of char, and so on. In this study, the FAP–HNT acted as a catalyst and a gas source to form an expanded charred layer; this was significant in the protection of the underlying materials from further pyrolysis and burning.[35] However, the gas source was not sufficient for the expansion and viscosity of the melt; that is, the formula of the EP composites also needed to be adjusted further.

The IR spectrum of the EP/FAP–HNT char [Figure 14(2)] presented a marked peak at 2919 cm^{-1}, which belonged to the C—H stretching in the EP groups. Different bands were observed around 3620 and 3695 cm^{-1} in the FTIR spectra of the FAP–HNT [Figure 14(1)] and the char of EP/FAP–HNT; these bands were attributable to the Al—OH stretching. Other marked peaks of the FAP–HNTs were located at 1626, 1422, and 1031 cm^{-1}. The band corresponding to the OH stretching of lattice water related to silicates also appeared around 3450 cm^{-1} in the FAP–HNTs as well as the absorption band due to free hydroxyl groups around 3630 cm^{-1} [Figure 14(1)]. This behavior was also observed in the FTIR spectrum of the EP/FAP–HNT (20) [Figure 14(2)]. In addition, the marked peaks of EP/FAP–HNT (20) were also located at 1597, 1453, 1147, 777, and 450 cm^{-1}. The band associated with free FAP–HNT hydroxyl groups in the EP/FAP–HNT (20) (3630 cm^{-1}) disappeared; this confirmed the formation of hydrogen bonds between the FAP–HNTs and —OH groups of the cured EP.[36]

Mechanical Properties

The FAP–HNTs contained HNTs and FAP, which are both inorganic nanofillers for polymers. The HNTs had a high mechanical strength and modulus and easy dispersability, and these features made it an ideal material for EP.[37] HNTs are effective additives for increasing the fracture toughness of cured epoxies without a sacrifice of their basic properties.[38] For comparative

Table VIII. Mechanical Properties of the EP Nanocomposites

Specimen	Tensile strength (MPa)	Elongation at break (%)	Tensile modulus (GPa)
Neat EP	31.4 ± 0.3	5.82 ± 0.4	2.87 ± 0.11
EP/HNT (20)	33.9 ± 0.8	4.50 ± 0.1	1.34 ± 0.06
EP/OP (5)	24.2 ± 0.5	2.58 ± 0.1	1.65 ± 0.03
EP/OP (10)	29.7 ± 0.4	4.30 ± 0.1	1.43 ± 0.10
EP/OP (20)	32.5 ± 0.5	2.61 ± 0.3	1.71 ± 0.03
EP/FAP/OP (5)	15.4 ± 0.2	5.30 ± 0.2	0.85 ± 0.12
EP/FAP/OP (10)	27.4 ± 0.3	2.47 ± 0.3	1.79 ± 0.07
EP/FAP/OP (20)	29.0 ± 0.1	3.75 ± 0.3	1.55 ± 0.04
EP/FAP-HNT/OP (5)	35.3 ± 0.2	3.02 ± 0.4	1.85 ± 0.09
EP/FAP-HNT/OP (10)	35.8 ± 0.4	2.89 ± 0.3	1.67 ± 0.06
EP/FAP-HNT/OP (20)	37.6 ± 0.6	3.97 ± 0.2	1.69 ± 0.12

analysis of the mechanical properties, the EP/OPs, EP/FAP–HNTs, and EP/OP/FAP–HNTs were tested by a tension testing system, and the results of the tensile strength, elongation at break, and tensile modulus are tabulated in Table VIII. It was evident that the elongation at break values of the EP composites were lower than that of neat EP. As the loading of additives increased from 5 to 20 wt %, the tensile strength for all of the EP composites increased.[39] With the addition of 20 wt % flame retardant, the tensile strengths of EP/HNT (20), EP/OP (20), EP/FAP/OP (20), and EP/FAP–HNT/OP (20) were 33.9 ± 0.8, 32.5 ± 0.5, 29.0 ± 0.1, and 37.6 ± 0.6 MPa, respectively. In a comparison with these data, the EP/FAP–HNT/OP (20) exhibited the highest tensile strength; this indicated a mechanical synergy of the FAP, HNTs, and OP. The EP/FAP–HNT/OP (5) (containing 1.25 wt % HNTs) showed the highest value of modulus. The use of HNTs in combination with FAP and OP produced a further improvement in the mechanical properties. Nakamura *et al.*[40] reported the effects of the HNT loading (2%) in EP resin on its mechanical properties. The Young's modulus of the EP nanocomposites increased slightly up to a loading of 0.25%, after which it started to decrease. This might have been related to the nanotube shape, size, and clustering. In this study, the trend of modulus was consistent with this literature. With increasing HNT loading in the EP/FAP–HNT/OP composites, the UTS slightly increased, possibly because of the interfacial adhesion between the HNTs and EP, along with uniformly dispersed HNTs and FAP in the EP matrix, which provided better stress transfer from the matrix to the reinforcing nanomaterial. Another possible reason was that the surface of the HNTs was improved by the FAP nanoparticles, so this enhanced the UTS of this formula to some extent. This was also verified by SEM and TEM analyses.

CONCLUSIONS

To recycle N and P from wastewater and lower the cost of flame retardants, we performed a study on the synthesis and application of FAP–HNT nanocomposites, a halogen-free inorganic flame retardant. The products were characterized by FTIR spectroscopy, SEM/EDS, TGA, and TEM. MCC, UL-94, and a tension testing system were used to determine the flame retardancy and mechanical properties of the EP/FAP–HNT in combination with Exolit OP. We found that the optimal conditions for the synthesis of the FAP–HNTs were as follows: a reaction time of about 30–40 min, a reaction temperature from room temperature to 80°C, a pH of about 9.5, a $Fe^{2+}/NH_4^+/PO_4^{3-}$ molar ratio of 1.4:1:1, and an HNT concentration of 1.9–19.5 mmol/L. The diameter of the HNT was about 200 nm, and that of the FAP particles was about 20–30 nm in the FAP–HNTs. The FTIR spectra demonstrated that a small amount of water in the FAP–HNTs acted as a catalyst for the curing reaction. The addition of FAP–HNT/OP (20 wt %) gave rise to a 39% reduction in HRR and about a 55 s PBT for EP. The EP/FAP–HNT/OP (20) passed the UL 94 V-0 rating. The analysis of the char revealed a synergy of the FAP–HNTs and OP in reducing the flammability of the polymers. The FAP–HNTs acted as a catalyst and a gas source during combustion, and the condensed phase flame-retarding mechanism played a key role in the fire resistance. EP/FAP–HNT/OP (20) also exhibited the highest tensile strength because of the mechanical synergy of the FAP, HNTs, and OP. We concluded that these nanocomposites show potential for applications in wastewater treatment and N/P recycling.

ACKNOWLEDGMENTS

The authors thank the Priority Academic Program Development of Jiangsu (China) Higher Education Institutions (contract grant number JHB2012-48) and Jiangsu Key Laboratory for Environment Functional Materials (contract grant number SJHG1306) for financial support.

REFERENCES

1. Sun, F.-Y.; Wang, X.-M.; Li, X.-Y. *Proc. Biochem.* **2013**, *48*, 1749.
2. Montalvo, S. J.; Guerrero, L. E.; Milán, Z. *J. Environ. Sci. Heal. A Toxic/Hazard. Subs. Environ. Eng.* **2011**, *46*, 1385.
3. Nieves, B.; Claudio, A.; José, A. S.; Beatriz, R.; Aŕanzazu, E.; José, R. G. *Thermochim. Acta* **2006**, *441*, 89.
4. Pana, B.; Wu, J.; Pan, B.; Lv, L.; Zhang, W.; Xiao, L.; Wang, X.; Tao, X.; Zheng, S. *Water Res.* **2009**, *43*, 4421.
5. Zheng, Y.; Wang, A. *J. Macromol. Sci. Pure Appl. Chem.* **2010**, *47*, 33.
6. Zhao, Y.; Abdullayev, E.; Vasiliev, A.; Lvov, Y. *J. Colloid. Int. Sci.* **2013**, *406*, 121.
7. Serge, B.; Sophie, D. *J. Mater. Chem.* **2007**, *17*, 2283.
8. Marney, D. C. O.; Russell, L. J.; Wu, D. Y.; Nguyen, T.; Crammb, D.; Rigopoulos, N.; Wright, N.; Greaves, M. *Polym. Degrad. Stab.* **2008**, *93*, 1971.
9. Liu, M.; Bao, G.; Du, M.; Lei, Y.; Jia, D. *J. Polym. Res.* **2008**, *15*, 205.
10. Du, M.; Guo, B.; Jia, D. *Polym. Int.* **2010**, *59*, 574.
11. Tang, Y.; Deng, S.; Ye, L.; Yang, C.; Yuan, Q.; Zhang, J.; Zhao, C. *Compos. A* **2011**, *42*, 345.
12. Alamri, H.; Low, I. M. *Polym. Compos.* **2012**, *33*, 589.
13. Marney, D. C. O.; Yang, W.; Russell, L. J.; Shen, S. Z.; Nguyen, T.; Yuan, Q.; Varley, R.; Li, S. *Polym. Adv. Technol.* **2012**, *23*, 1564.
14. Liu, Y.; Kumar, S.; Kwag, J.-H.; Ra, C. *J. Chem. Technol. Biotechnol.* **2013**, *88*, 181.
15. Rawtani, D.; Agrawa, Y. K. *Rev. Adv. Mater. Sci.* **2012**, *30*, 282.
16. Erskine, A. M.; Grim, G.; Horning, S. C. *Ind. Eng. Chem.* **1944**, *36*, 456.
17. Pier, P. P.; Paola, G.; Cinzia, C.; Maria, C.; Amedeo, M. *Mater. Res. Bull.* **2013**, *48*, 3438.
18. Vol'fkovich, S. I.; Remen, R. E. *Chem. Abstr.* **1956**, *50*, 6243.
19. Ricciardi, M. R.; Antonucci, V.; Giordano, M.; Zarrelli, M. *J. Fire Sci.* **2012**, *30*, 318.
20. Garrell, M. G.; Shih, A. J.; Lara-Curzio, E.; Scattergood, R. O. *J. Test. Eval.* **2003**, *31*, 52.
21. Boudin, S.; Lii, K.-H. *Inorg. Chem.* **1998**, *37*, 799.
22. Stefova, V.; Šoptrajanov, B.; Spirovski, F.; Kuzmanovski, I.; Lutz, H. D.; Engelen, B. *J. Mol. Struct.* **2004**, *689*, 1.

23. Gürbüz, H.; Tokay, B.; Erdem-Senatalar, A. *Ultrason. Sonochem.* **2012**, *19*, 1108.
24. Choi, S.; Janisse, A. P.; Liu, C.; Douglas, E. P. *J. Polym. Sci. Part A: Polym. Chem.* **2011**, *49*, 4650.
25. Liu, M.; Guo, B.; Du, M.; Cai, X.; Jia, D. *Nanotechnology* **2007**, *18*, 455703.
26. Beatriz, R.; Aranzazu, E.; Nieves, B.; José, R. G. *Thermochim. Acta* **2009**, *487*, 60.
27. Wang, X.; Song, L.; Yang, H.; Xing, W.; Kandola, B.; Hu, Y. *J. Mater. Chem.* **2012**, *22*, 22.
28. Gracik, T. D.; Long, G. L. *Thermochim. Acta* **1992**, *212*, 163.
29. Lu, S.-Y.; Hamerton, I. *Prog. Polym. Sci.* **2002**, *8*, 1661.
30. Alhuthali, A. M.; Low, I. M. *J. Reinf. Plast. Compos.* **2012**, *32*, 233.
31. Liu, M.; Guo, B.; Du, M.; Jia, D. *Appl. Phys. A: Mater. Sci. Proc.* **2007**, *88*, 91.
32. Wang, Y.; Zhang, J.; Jow, J.; Su, K. *J. Fire Sci.* **2009**, *27*, 561.
33. Cogen, J. M.; Lin, T. S.; Lyon, R. E. *Fire Mater.* **2009**, *33*, 33.
34. Du, M.; Guo, B.; Jia, D. *Eur. Polym. J.* **2006**, *42*, 1362.
35. Koo, J. H. Polymer Nanocomposites: Processing, Characterization, and Applications; McGraw-Hill: New York, **2006**.
36. Mondragón, M.; Cortes, M. A.; Arias, E.; Falcony, C.; Zelaya-Angel, O. *Polym. Eng. Sci.* **2011**, *51*, 1808.
37. Rawtani, D.; Agrawal, Y. K. *Rev. Adv. Mater. Sci.* **2012**, *30*, 282.
38. Tang, Y.; Deng, S.; Ye, L.; Yang, C.; Yuan, Q.; Zhang, J.; Zhao, C. *Compos. A* **2011**, *42*, 345.
39. Tang, Y.; Ye, L.; Deng, S.; Yang, C.; Yuan, W. *Mater. Des.* **2012**, *42*, 471.
40. Nakamura, R.; Netravali, A. N.; Hosur, M. V. *J. Adhes. Sci. Technol.* **2012**, *26*, 1295.